Effect of lithium on the properties of a liquid crystal formed by sodium dodecylsulphate and decanol in aqueous solution

ARTICLE *in* THE JOURNAL OF CHEMICAL PHYSICS · JULY 2013

Impact Factor: 2.95 · DOI: 10.1063/1.4811678 · Source: PubMed

6 AUTHORS, INCLUDING:

Jose Javier Lopez Cascales
Universidad Politécnica de Cartagena
62 PUBLICATIONS **774** CITATIONS
SEE PROFILE

Rodrigo Montecinos
Pontifical Catholic University of Chile
14 PUBLICATIONS **50** CITATIONS
SEE PROFILE

Ramiro Araya-Maturana
Universidad de Talca
92 PUBLICATIONS **474** CITATIONS
SEE PROFILE

Effect of lithium on the properties of a liquid crystal formed by sodium dodecylsulphate and decanol in aqueous solution

V. E. Bahamonde-Padilla, Javier Espinoza, B. E. Weiss-López, J. J. López Cascales, R. Montecinos et al.

Citation: J. Chem. Phys. **139**, 014703 (2013); doi: 10.1063/1.4811678
View online: http://dx.doi.org/10.1063/1.4811678
View Table of Contents: http://jcp.aip.org/resource/1/JCPSA6/v139/i1
Published by the AIP Publishing LLC.

Effect of lithium on the properties of a liquid crystal formed by sodium dodecylsulphate and decanol in aqueous solution

V. E. Bahamonde-Padilla,[1] Javier Espinoza,[1] B. E. Weiss-López,[1,a)]
J. J. López Cascales,[2,a)] R. Montecinos,[3] and R. Araya-Maturana[4]
[1]*Departamento de Química, Facultad de Ciencias, Universidad de Chile, Casilla 653, Santiago, Chile*
[2]*Grupo de Bioinformatica y Macromoleculas (BioMac), Universidad Politécnica de Cartagena, Area de Química Física, Aulario II, Campus de Alfonso XIII, 30203 Cartagena, Murcia, Spain*
[3]*Facultad de Química, Pontificia Universidad Católica de Chile, Av. Vicua Mackenna 4860, Santiago, Chile*
[4]*Facultad de Ciencias Químicas y Farmaceúticas, Universidad de Chile, Casilla 233, Santiago 1, Chile*

(Received 20 February 2013; accepted 23 May 2013; published online 2 July 2013)

Understanding the molecular interactions that rule the physicochemical properties of molecular assemblies is of particular interest when trying to explain the behavior of much more complicated systems, such as the cell membranes. This work was devoted to study a discotic nematic lyotropic liquid crystal, formed by sodium dodecylsulphate (3% SDS-d_{25}) and decanol (20% DeOH-α-d_2), dissolved in aqueous solutions (0.1% D_2O) of Na_2SO_4 or Li_2SO_4. The average size of the aggregates was estimated using fluorescence quenching experiments, and their dynamics were studied by measuring the ^{2}H-NMR quadrupole splitting ($\Delta\nu_Q$) and the longitudinal relaxation times (T_1) of the deuterated species. To provide an atomic insight into these assemblies, molecular dynamics simulations of the systems were carried out with atomic detail. As a previous step in this study, a reparameterization of the standard GROMOS 87 force field was required to perform the equilibrated simulations and to prevent instabilities emerging during the simulations. Finally, an excellent agreement between simulation and experimental data was obtained. In addition, variations in the long range electrostatic interactions at the aggregate/solution interface, the orientation and the reorientational relaxation time of the water dipole, the translational diffusion coefficient of sodium ions, and the amphiphile-counterion coordination associated with the presence of Li^+ in the solution were other key aspects investigated to explain the variation in the quadrupole splittings ($\Delta\nu_Q$) in the presence of lithium in solution. © *2013 AIP Publishing LLC*. [http://dx.doi.org/10.1063/1.4811678]

I. INTRODUCTION

Ionic amphiphiles dissolved in water spontaneously aggregate to form a variety of different structures. At constant temperature and pressure, the characteristics of the aggregates depend on the nature and concentration of the amphiphile, its counterion, the presence of other components, and the solvent. At moderate concentrations, above the Critical Micelle Concentration (CMC), isotropic micelles are formed. If the amphiphile concentration is increased, anisotropic liquid crystal phases, such as lamellar and hexagonal assembles (among others), appear. Furthermore, by adding long chain aliphatic alcohols and increasing the ionic strength of the aqueous solution by the addition of salt, two types of nematic lyotropic liquid crystals (NLLCs) of finite size can be generated: calamitic (NC), derived from the hexagonal phase with prolate symmetry, and discotic (ND), derived from the lamellar phase with oblate symmetry.[1–6] Despite their structural differences, all these systems show three characteristic regions: (i) the aqueous phase, containing a small amount of free amphiphiles and ions dissolved, (ii) the interface, where the most important electrostatic interactions between head-groups, ions, and water occur, and (iii) the hydrophobic core, formed by hydrocarbon chains. These three regions are also found in the bilayer structure of eukaryotic cell membranes, where interactions in the interfacial region play a critical role determining the curvature of this region, which strongly affects the size and shape of the aggregates.[7,8] Hence, a deeper knowledge of the molecular interactions that govern the physicochemical processes of these relatively simple molecular assemblies will contribute to a better understanding of more complicated structures, such as those of biological membranes.

Furthermore, the bilayer arrangement displayed by Discotic Lyotropic Liquid Crystals (DLLCs), combined with their capacity to be orientated in the presence of magnetic fields, means they can be considered as simple membrane models, particularly suitable for study by nuclear magnetic resonance (NMR).[9] Recently, nematic lyotropic liquid crystals in combination with magnetic fields have been used in the synthesis of carbon nanotubes with a given preferential orientation, since their orientation can be controlled by the magnetic field applied to the system. They have also been used as templates for the synthesis of nanowires and for the generation of meso-structured materials.[10–14]

In this work we present an experimental study on the size, structure, and dynamics of two discotic nematic lyotropic liquid crystals. The sample denoted as S1 was prepared by dissolving sodium dodecylsulphate (10% SDS-d_{25}) and decanol (DeOH-α-d_2) in an aqueous solution containing

a)Authors to whom correspondence should be addressed. Electronic addresses: bweiss@uchile.cl and javier.lopez@upct.es

Na_2SO_4 (0.1% D_2O). In the second sample, S2, the solution of Na_2SO_4 was substituted by a solution of identical concentration of Li_2SO_4. The molecular aggregate sizes were estimated from static fluorescence quenching measurements of added pyrene by *N*,*N*-dimethylaniline (DMA), and their dynamics was studied based on ^{2}H-NMR quadrupolar splitting measurements and longitudinal relaxation times. Furthermore, with the aim of gaining insight into the behavior of these aggregates at molecular level, molecular dynamics (MD) simulations of simple aggregate models were carried out at an atomic level.

From a biophysical point of view, the interest of studying the effect of Li^+ on these aggregates with net negative charge (which resemble the cell membranes of the central nervous system that are mainly composed of PS with also a net negative charge in physiological conditions[15]) arises from the fact that Li^+ has been widely used as a therapeutic agent for over 60 years[16] in the treatment of certain mental diseases related with manic depressive disorders. Thus, a significant amount of information on the effects of Li^+ ions in different processes of living organisms has been collected.[17–22] However, and despite the huge amount of pharmacological information available in the bibliography, the molecular mechanism by which Li^+ is able to produce therapeutic effects remains unknown. Recent studies have shown that Li^+ increases neuronal membrane excitability and decreases the slope of the decay after hyper-polarization, which is consistent with an interference on the part of Li^+ in the activation of the I-K^+-Na^+ channels.[23] Hence, it was thought that a study at molecular level of the differences in dynamics, distribution, and interaction between Na^+ and Li^+ in aqueous solution using a simple model of a cell membrane in its liquid crystalline phase might provide important information for understanding the actuation mechanism of lithium ions at molecular level, and how this is related with its biological activity.

II. METHODS AND MODELS

A. Experimental work

1. Mesophase preparation and NMR spectra

SDS (>99%) was purchased from Aldrich and crystallized from the ethanol/ethyl acetate mixture before being used. SDS-d_{25} was purchased from Aldrich and used as received. The water to prepare the samples was of high-performance liquid chromatography grade, from Merck. All the other reagents (from Aldrich) were of the highest purity available and were used as received. The liquid crystal solutions with Na_2SO_4 were prepared by dissolving 0.514 g of SDS, 0.010 g of SDS-d_{25}, 0.0473 g of Na_2SO_4, and 0.108 ml of decanol in 1 ml of water (sample S1, corresponding to 0.30 M in Na_2SO_4). The second sample was prepared by replacing the Na_2SO_4 by 0.0433 g of Li_2SO_4 (sample S2, in 0.35 M Li_2SO_4). Both mesophases were allowed to equilibrate at least 24 hours at 310 K before measurements were made.

All NMR spectra were obtained at 310 K in a Bruker Avance 400 NMR spectrometer, located at the University of Santiago of Chile, using a broadband probe tuned to 61.425 MHz. Deuterium longitudinal relaxation times were obtained using the T1IR pulse sequence. The ^{2}H 90° pulse was 19 μs and more than 1000 transients from a spectral window of 40 kHz were accumulated in 32 kB files.

2. Fluorescence spectroscopy

Pyrene (99%) and *N*,*N*-dimethylaniline were purchased from Aldrich and used as received. A series of steady-state fluorescence spectra of pyrene quenched by different concentrations of DMA allows an estimate of the aggregation number, i.e., the number of amphiphiles (SDS+DeOH) that form the micelle.[5,24,25] Five microlitres (5 μl) of a 4×10^{-3} M solution of pyrene in acetonitrile was deposited in a 10 ml flask; after solvent evaporation, 5 ml of mesophase was added. This solution was homogenized and poured in 5 tubes with 1 ml each. A volume of 0.0, 0.5, 1.0, 1.5, and 2.0 μl of pure DMA was added to the above mentioned tubes and allowed to equilibrate for 48 hours at 310 K. Fluorescence spectra from these samples were recorded using a LS-55 Perkin-Elmer spectrofluorometer. The basis of the method assumes a Poisson distribution of the quencher (DMA) within the aggregates. Each aggregate can include a maximum of one pyrene and one DMA molecule, and any emission must only be from pyrene. The results of these experiments are $nS1 = 246 \pm 22$ units and $nS2 = 227 \pm 26$ units. The errors were obtained from 3 different measurements. It is well known that aggregation numbers obtained using the steady state quenching methodology underestimate the value of n;[26] however, this methodology is sufficient for the comparative purposes of this study.

B. Simulation parameters

The package GROMACS 3.3.3[27,28] was used to perform the molecular dynamics simulations, although most of the analysis carried out in this work was performed using our own code. The molecular aggregates were simulated as bilayers containing 156 molecules (78 per leaflet) of Sodium-DodecylSulphate SDS^- (see Figure 1) and 156 Na^+ to balance the net charge associated with each SDS molecule, 40 decanol molecules (20 DeOH molecules per leaflet) (see Figure 1), 2633 H_2O molecules, and 10 units of Na_2SO_4 or Li_2SO_4, corresponding to a concentration of 0.5 M in Na^+ or Li^+. Periodic boundary conditions were considered along the three-dimensional space, and the simulation integration time step was of 2 fs. Figure 2 shows a schematic representation of the computational box and how the amphiphiles are oriented with respect to the magnetic field, $\vec{B}$.

The long range electrostatic contribution was calculated using the Particle Mesh Ewald method[29,30] with a cutoff of 1 nm. Bond lengths were constrained using LINear Constraint Sonvent algorithm (LINCS).[31] The systems were coupled to an external pressure and temperature bath, using the Berendsen algorithm,[32] with temperature and pressure coupling constants of 0.1 and 1 ps, respectively. Due to the anisotropy in the molecular assembly, all the simulations were carried out under a semi-isotropic pressure coupling bath. The simulated trajectories were 100 ns long, and the coordinates of all the atoms of the systems were recorded every 1 ps of

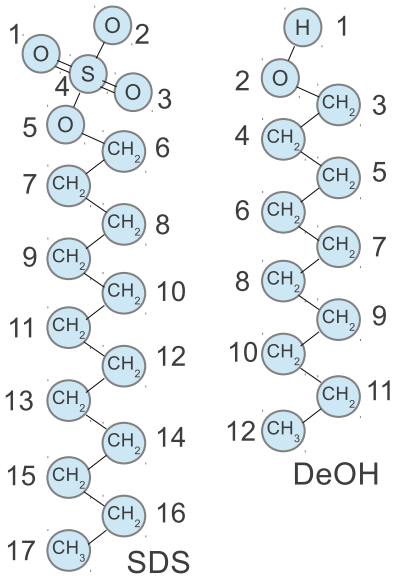

FIG. 1. Atomic numeration of SDS and DeOH used in this work.

simulation time. All the simulations were carried out at 310 K. The charge distributions of all the species involved in our simulations are depicted in Table I. The charge distributions of SDS and DeOH were obtained using the semi-empiric Complete Neglect of Differential Overlap (CNDO) method,[33] and the charges of sulphate SO_4^{-2} were obtained from *ab initio* calculations, using the 6-31G* basis set and MK fitting.[34,35] However, for achieving an equilibrated state, the charges of all the species bearing a net charge had to be halved, if this was not done, the systems collapsed or exploded after a few nanoseconds of simulation time. In this respect several physicochemical reasons justify this charge reduction, which has been discussed elsewhere.[36–41] These reasons include the absence of polarizability of all the species involved in the simulation (mainly the solvent) or the vacuum permittivity in the MD simulations, where any of these factors will contribute to an overestimation in the values of the electrostatic interactions.

Table II shows the modified Lennard-Jones parameters used in our simulations, as proposed by Egberts

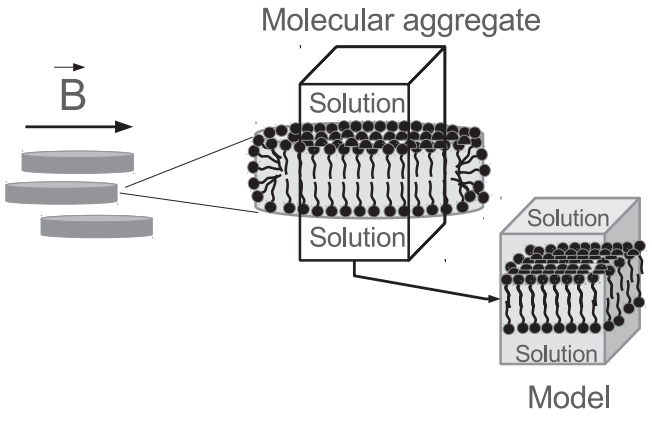

FIG. 2. Schematic representation of the bilayer model used in our study, resembling the structure of a molecular aggregate whose boundary effects were discarded in our simulations.

TABLE I. Atomic charge distribution for all the species involved in the simulations. The SDS and DeOH charge distributions were obtained by the semi-empiric CNDO method,[33] and the SO_4 charge distribution from *ab initio* 6-31G calculations. The atomic numeration for SDS and DeOH matches the corresponding numeration in Figure 1.

SDS			DeOH		
Atom number	Type	Charge (e)	Atom number	Type	Charge (e)
1	OM	− 0.404	1	H	0.426
2	OM	− 0.404	2	OS	− 0.722
3	OM	− 0.404	3	CH_2	0.329
4	S	0.444	4	CH_2	− 0.033
5	OS	− 0.286	5	CH_2	0.000
6	CH_2	0.108	6	CH_2	0.000
7	CH_2	− 0.028	7	CH_2	0.000
8	CH_2	0.000	8	CH_2	0.000
9	CH_2	0.000	9	CH_2	0.000
10	CH_2	0.000	10	CH_2	0.000
11	CH_2	0.000	11	CH_2	0.000
12	CH_2	0.000	12	CH_3	0.000
13	CH_2	0.000		Ions	
14	CH_2	0.000		Na^+	1.00
15	CH_2	0.000		Li^+	1.00
16	CH_2	0.000		$S(SO_4^{-2})$	1.504
17	CH_3	0.000		$O(SO_4^{-2})$	− 0.876

et al.,[37] based on GROMOS 87 standard force field.[42] The water model used in our simulation was the Simple Point Charge (SPC).[43] In this regard, Figure 3 shows the running surface area per SDS molecule during 100 ns of simulation time. In further analyses in this work (below), the first 10 ns of any simulation were discarded because this time was the equilibration time needed by the systems. Thus, from the last 90 ns of simulation, mean surface areas of 0.356 ± 0.006 and 0.340 ± 0.005 nm^2 per SDS molecule were calculated for the S1 and S2 samples, respectively.

III. RESULTS AND DISCUSSION

A. Phase characterization of the molecular aggregates

In a preliminary attempt to confirm that samples S1 and S2 were in a discotic nematic liquid crystal phase (DNLCP), an exploratory study was made of the phase diagrams of both

TABLE II. Lennard-Jones parameters involved in our simulations, considering the potential equation $V = 4\epsilon((\frac{\sigma_{ij}}{r_{ij}})^{12} - (\frac{\sigma_{ij}}{r_{ij}})^{6})$.

Atom type	σ (Å)	ϵ (kJ/mol)
H	0	0
OM	2.9603	0.8772
S	3.3077	1.9056
OS	2.6259	1.7246
CH_2	3.9598	0.3800
CH_3	3.9600	0.5699
Na^+	2.5750	0.0617
Li^+	1.5442	26.1404
OW	3.1654	0.65032
HW	0	0

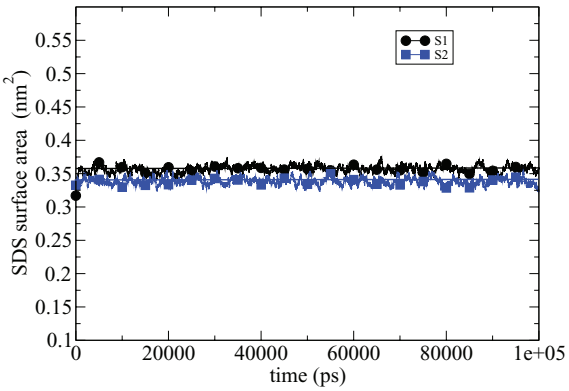

FIG. 3. Mean surface area per SDS molecule of the simulated bilayers, corresponding to the S1 and S2 samples in the absence and presence of lithium, respectively.

samples, using polarized light microscopy textures. Thus, by increasing and decreasing the concentration of each component by 10% with respect to their original concentrations, 8 additional samples were prepared. Figure 4 shows the textures of a sample of S1 and S2, once they were orientated in the magnetic field. From a visual comparison with experimental textures previously reported in the literature,[44,45] it was confirmed that the samples were in their discotic nematic mesophase. In the same way, all the samples explored in this preliminary study showed that S1 and S2 were in the discotic nematic region of the phase diagrams. Furthermore, we made a thermal stability study of both samples, starting from 45 °C (a temperature at which the texture of both samples is characteristic of discotic nematics) before cooling to 10 °C. In this regard, sample S1 showed clear signs of precipitation below 30 °C, while sample S2 remained intact over the whole range of temperatures investigated down to 10 °C when it precipitated. Hence, these results confirmed that we are looking at samples S1 and S2 in their discotic nematic liquid crystal phase.

B. ^{2}H-NMR quadrupolar splitting study

Figure 5 shows the ^{2}H-NMR spectrum of the S1 and S2 samples. The smallest splitting is associated with DHO and the largest with DeOH-α-d_2. Intermediate splittings in between come from SDS-d_{25}. The values of $\Delta\nu_Q$ measured directly from the spectra were assigned on the basis of their relative intensities and the fact that the most mobile C–D bond shows the smallest splitting and the longest relaxation time, T_1.[46] Significant overlaps (and hence only one peak) were observed for the largest splittings, and accordingly, only one frequency was assigned to each group. Table III shows all the experimentally obtained data of $\Delta\nu_Q$ for the SDS molecule in the aggregate.

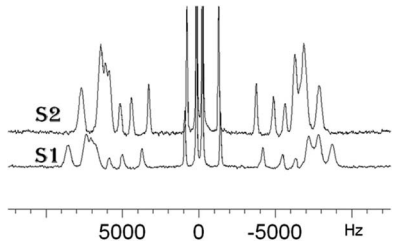

FIG. 5. ^{2}H-NMR spectra of S1 and S2 samples.

A deeper inspection of Table III reveals that in both mesophases there are regions with a similar degree of alignment for the aliphatic chain of SDS, i.e., regions with similar mobility. We found the most rigid region of the bilayer from C_1 to C_4, while from C_5 to C_6 and C_7 to C_8 there were two sectors of increasing mobility, and the alignment for the rest of the chain decreased systematically from C_9 to C_{12}. Furthermore, Table III shows that all $\Delta\nu_Q$ for S2 are roughly 10% smaller than $\Delta\nu_Q$ for S1. Replacing Na_2SO_4 by Li_2SO_4 in the aqueous solution decreased the degree of alignment of the complete SDS aliphatic chains with the magnetic field. In line with the above comments, a plot of the difference ($\Delta\nu_Q(S1) - \Delta\nu_Q(S2)$) versus the carbon atom number of the SDS aliphatic chain is displayed in Figure 6. This figure shows a clear discontinuity from C_4 to C_5, which strongly suggests that the main effect of Li^+ on the bilayer structure is on the mobility of the first few carbon atoms of the SDS chain, i.e., near the interface (just next to the amphiphile head). This is not a surprising result, considering that in this type of system the counterions are well represented in this region.

These observations are in a perfect agreement with previous studies on the Li^+ effects on human erythrocytes and membrane models of dimyristoylphosphatidylcholine (DMPC) and dimyristoylphosphatidylethanolamine

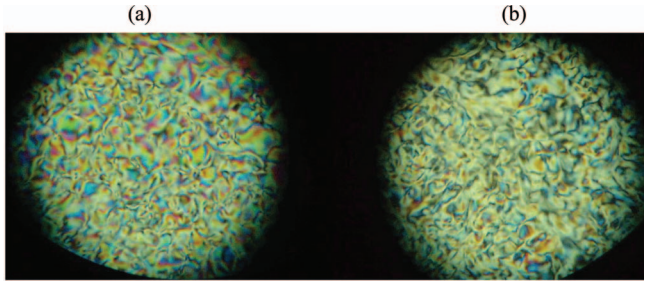

FIG. 4. Polarized light microscopy texture of magnetic field orientated samples S1 (a) and S2 (b). A comparison of these textures with previous reported textures of DNLLC in similar systems[45,46] allows us to conclude that S1 and S2 are DNLLCs.

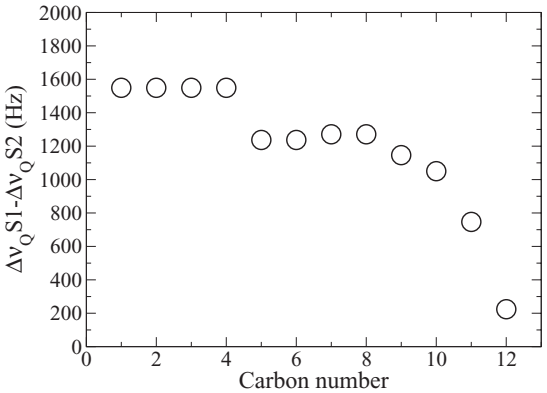

FIG. 6. Differences in quadrupolar splitting ($\Delta\nu_Q(S1) - \Delta\nu_Q(S2)$) vs. carbon number of the SDS aliphatic chain.

TABLE III. Experimental and simulation ^{2}H quadrupolar splitting ($\Delta\nu_Q$) in Hz, relaxation time T_1 in ms for DHO and SDS-d_{25}, for the samples S1 (without lithium) and S2 (with lithium).

	$\Delta\nu_Q$ $S1^{exp}$	$\Delta\nu_Q$ $S1^{sim}$	T_1 S_1	$\Delta\nu_Q$ $S2^{exp}$	$\Delta\nu_Q$ $S2^{sim}$	T_1 S2	$\Delta(\Delta\nu_Q)$
DH0	393 ± 4		432 ± 5	395 ± 4		432 ± 5	
C_1	15142 ± 60	14573 ± 128	48 ± 15	13593 ± 60	13770 ± 64	47 ± 14	1549
C_2	15142 ± 60	13999 ± 242	48 ± 15	13593 ± 60	13132 ± 77	47 ± 14	1549
C_3	15142 ± 60	13961 ± 217	48 ± 15	13593 ± 60	13005 ± 102	47 ± 14	1549
C_4	15142 ± 60	14445 ± 242	48 ± 15	13593 ± 60	13387 ± 64	47 ± 14	1549
C_5	14500 ± 60	14280 ± 179	60 ± 11	13263 ± 60	13132 ± 127	53 ± 12	1237
C_6	14500 ± 60	14063 ± 166	60 ± 11	13263 ± 60	12750 ± 77	53 ± 12	1237
C_7	13868 ± 70	13387 ± 179	63 ± 11	12597 ± 70	11985 ± 77	55 ± 11	1271
C_8	13868 ± 70	12533 ± 464	63 ± 11	12597 ± 70	11092 ± 77	55 ± 11	1271
C_9	12191 ± 60	11067 ± 77	62 ± 7	11045 ± 60	9690 ± 77	74 ± 8	1146
C_{10}	10496 ± 40	9218 ± 1285	90 ± 7	9446 ± 30	7905 ± 77	96 ± 5	1050
C_{11}	7891 ± 40	6604 ± 64	149 ± 5	7144 ± 30	5482 ± 64	154 ± 5	747
C_{12}	2337 ± 10		406 ± 5	2113 ± 10		384 ± 4	224

(DMPE).[22] Using X-ray diffraction data and fluorescence spectroscopy, these authors observed that Li^+ induces important structural perturbations on the polar head-groups of the acyl regions in DMPC and DMPE bilayers. Furthermore, fluorescence depolarization experiments performed on DMPC large unilamellar vesicles show that Li^+ interacts with the lipid polar head-groups and increases the mobility of the hydrophobic acyl chains.

In charged bilayers of dipalmitoylphosphatidylserines (DPPS), the incorporation of Li^+ induces the formation of DPPS micro-crystals, and thus, a significant increase in the enthalpy and transition temperature from this *crystalline phase* to a more ordered one[47,48] has been reported. Furthermore, MD simulations showed that Li^+ induces a phase transition from a liquid crystalline phase to a more ordered gel phase[48] in a DPPS bilayer. For the mesophases involved in this study, the replacement of Na^+ by Li^+ decreases the general degree of alignment with the magnetic field. This diminution in the orientation of the aggregate with the magnetic field has three possible origins:

1. Perturbation of the internal dynamics of the ethylene groups inside the aggregate.
2. A difference in size of the aggregate for the S1 and S2 systems.
3. A combination of both.

In order to investigate experimentally how the substitution of Na_2SO_4 by Li_2SO_4 affects the average size of the molecular aggregates, we measured the static fluorescence quenching of pyrene probes at different concentrations of *N*,*N*-dimethylaniline. In low occupancy conditions, these experiments provided an estimation of the number of aggregate units, i.e., the number of SDS-DeOH molecules that form each discotic micelle. This methodology, which can be applied to static and dynamic fluorescence, was originally developed for spherical micelles,[24] and later employed in nematic discotic lyotropic liquid crystals.[5,25] The results of these experiments provided 246 ± 22 and 227 ± 26 units for the aggregation numbers of the S1 and S2 samples, respectively. These values are in good agreement with the value of 236 ± 25 measured for similar SDS mesophase by Montecinos *et al.*[5] The observed difference in the aggregate size between S1 and S2 is within the experimental error. These experimental data are also in line with the values estimated from simulation for the surface area per SDS molecule, where values of 0.356 ± 0.006 and 0.340 ± 0.005 nm^2 were obtained for the S1 and S2 systems, respectively. This is evident how almost no variation in the surface area per SDS molecule was observed (i.e., in the total surface area of the micelles) at the concentrations of lithium involved in our study.

Hence, these results strongly suggest that the observed differences in $\Delta\nu_Q$ do not arise from differences in size in the micelles, and as a consequence, they must be attributable to differences in the internal dynamics of these aggregates, possibly due to different interactions between Li^+ and Na^+ with the aggregate.

1. Simulated order parameters, S_{CD}

In order to gain insight into the origin of the observed differences at an atomic scale, molecular dynamics simulations of the S1 and S2 samples were performed, and different properties were investigated to throw light on the diminishing quadrupolar splitting observed from the ^{2}H-NMR measurements.

In this regard, the order parameter, S_{CD}, is defined as

$$\langle S_{CD}\rangle = \frac{\langle 3\cos^2\phi - 1\rangle}{2}, \tag{1}$$

where ϕ corresponds to the angle between the C–D bond and the magnetic field, and the average is calculated along the simulation time for each ethylene of the hydrocarbon tail of the SDS molecule. Due to the fact that the ethylene groups were modelled as unit atoms in our simulations (see Figure 1), the C–H orientation cannot be calculated directly from the simulation. However, the order parameter corresponding to the *i*th carbon atom, C_i, can be obtained from the vector between C_{i+1} and C_{i-1}, and the vector perpendicular to this C_{i+1}–C_{i-1} which is contained in the C_{i+1}–C_i–C_{i-1} plane. Hence, this last vector will be employed to calculate the order parameter of the ethylene groups.

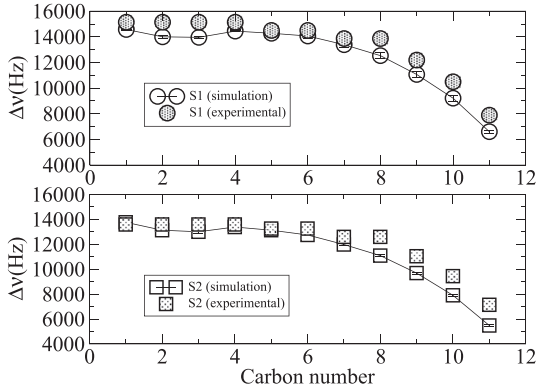

FIG. 7. Experimental and calculated quadrupole splitting for the samples S1 and S2.

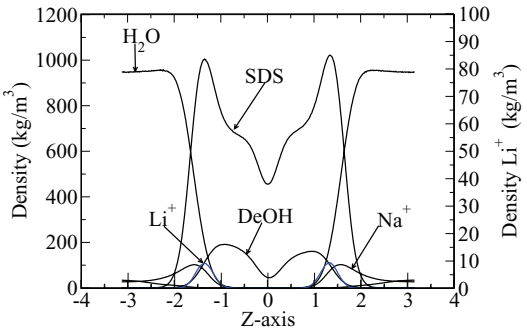

FIG. 8. Density profile along the z-axis normal to the aggregate surface for the components of the system S2. Zero axis was placed in the middle of the aggregate bilayer.

On the other hand, the quadrupole splitting, $\Delta\nu_Q$, obtained from ^{2}H-NMR measurements is related with the order parameters, S_{CD}, by the following expression:

$$\Delta\nu_Q = \frac{3}{4}A\langle S_{CD}\rangle, \tag{2}$$

where A is the quadrupole coupling constant (170 kHz)[49] and S_{CD} is the order parameter of a certain ethylene group. Thus, since the order parameters are proportional to the quadrupole splitting (simply multiplied by a constant), we will center our discussion on quadrupole splittings because these are quantities directly related with the experimental measurements.

Figure 7 shows a plot of the quadrupole splitting, measured from ^{2}H-NMR and simulation along the SDS aliphatic tail. From this figure, we appreciate the excellent agreement between both sets of data, both from a qualitative and quantitative point of view. The same Figure 7 points to an increase in disorder along the hydrocarbon tails from S1 to S2. These results can be considered as an excellent validation of the force field used in our simulations. The slight discrepancy existing between experimental and simulation data can be related with the finite size of the model used in our simulations, in which the boundary effects of the aggregate were discarded in our calculations.

C. Characterization of the molecular aggregate/solution interface

Figure 8 shows the mass distribution of the S2 sample obtained from simulation. All the density profiles are represented with respect to the left axis, except Li^+, which is represented in the right hand one, because their low values require a different axis escalation. The lithium distribution profile has a narrow shape, which means that the lithium ions are mainly located at fixed positions in the aggregate, unlikely the broad distribution of sodium ions, which means that sodium ions can be found from the bulk solution to the aggregate/solution interface. From these results, we deduce that Li^+ remains almost anchored to the aggregate.

In line with this result and bearing in mind that the Li^+ hydration radius is smaller than the corresponding one in Na^+,[50] lithium is able to penetrate deeper into the molecular aggregate. Thus, once lithium reaches these deep positions in the aggregate, the potential generated by other counterions and its own coordination with the SDS oxygens (which will be discussed below) will prevent lithium ions from diffusing into the aqueous solution. Therefore, the observed differences in $\Delta\nu_Q$ between S1 and S2 must be related with the location of the counterion at the interface.

In this context, we calculated the charge density distribution along the z-axis perpendicular to the surface of the aggregate (including the net charge associated with the water dipole orientation). Figure 9 shows the charge distribution profile of the different components analyzed. This figure shows an overlap between the positive charge distributions associated with water (due to the orientation of the water dipoles in the vicinity of the interface) and the Li^+ distribution; as a consequence, the electrostatic energy should be positive as would correspond to repulsive electrostatic interactions. Indeed, the calculated value of the short range electrostatic interactions between Li^+ and H_2O (using a 1 nm cutoff) was 183 kJ/mol (repulsive). In contrast, the calculated electrostatic interactions (including the sodium ions in the bulk) between Na^+ and H_2O provided a value of -9115 kJ/mol (attractive). Furthermore, the short range electrostatic interaction between SDS and counterions was -3079 kJ/mol for Na^+ compared with the value of -1699 kJ/mol for Li^+. And finally, the SDS head-group repulsion in the S1 was 825 kJ/mol, whereas in S2 it was 1028 kJ/mol. Hence, the substitution of Na_2SO_4 by Li_2SO_4 increases the electrostatic repulsions at the

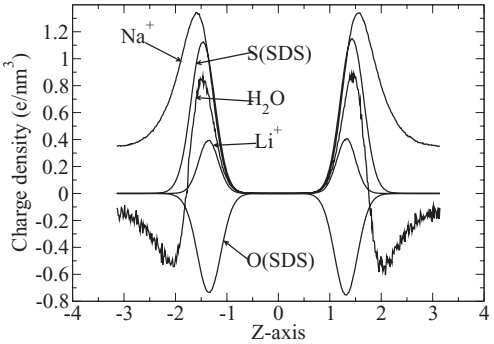

FIG. 9. Charge density along the z-axis normal to the aggregate surface of the system S2. Zero was located at the middle of the aggregate.

interface, and as a consequence, a decrease in the alignment of the components of the aggregate with the magnetic field is to be expected.

In this regard, and because lithium ions remain almost totally anchored to the aggregate during the whole simulation, important perturbations in the properties of the interface were observed compared with when only sodium was present in the aqueous solution. Thus, for a better characterization of how the interface is perturbed by the presence of lithium ions, the translational diffusion coefficient of sodium (the common counterion that is present in both samples), the coordination of sodium and lithium to the SDS, and the orientation and reorientational relaxation time of water dipole were investigated.

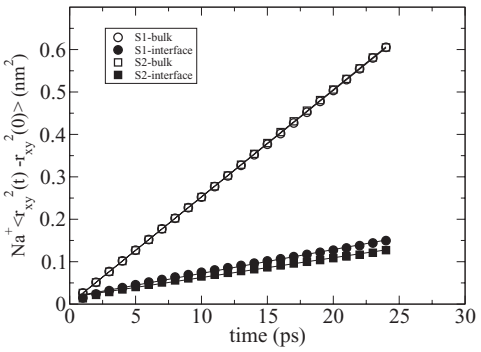

FIG. 10. Mean square displacement of sodium ions in bulk solution and at the aggregate/solution interface, corresponding to the samples S1 and S2 (in the absence and presence of lithium ions, respectively).

1. Sodium translational diffusion coefficient, D_t

To gain deeper insight into the effects of lithium on the interface properties, the translational diffusion coefficient of sodium was estimated in the bulk solution and at the interface, in view of the fact that sodium was the common counterion of the S1 and S2 samples.

The diffusion coefficient, D_t, was calculated from the mean square displacement, as follows:

$$\lim_{t\to\infty} \langle r^2(t)\rangle = 2f\,D_t t, \tag{3}$$

where r^2 is the square displacement of the center of mass, and the brackets mean the average over each type of ion, and f is the number of translational degrees of freedom considered in the motion. In our case, f will be equal to 2 (the perpendicular motion to the membrane plane will be discarded) because we are only interested in the lateral motion of the sodium in planes parallel to the aggregate face. In such a case, Eq. (3) becomes

$$\lim_{t\to\infty} \langle r_{xy}^2(t)\rangle = 4D_t t, \tag{4}$$

where r^2 is the squared displacement in a certain x, y layer of (typically) 0.5 nm thickness. Thus, and as a consequence of the high mobility of sodium ions, an ion may pass during the simulation time several times from one slab to a neighboring one. We solved this problem by splitting up the simulation trajectory into shorter subtrajectories of 25 ps each, in which each subtrajectory was assigned to the slab in which the center of mass of each ion (computed along the complete subtrajectory) resided. In this regard, Figure 10 shows the $r_{xy}^2(t)$ displacement of sodium in a slab of 0.5 nm thickness placed in the bulk solution and at a position Z corresponding to the maximum of the water dipole orientation of Figure 12, in the absence and presence of lithium ions.

From the fit of the displacements for sodium ions to a lineal regression in Figure 10, values of $6.2 \times 10^{-5}\,cm^2\,s^{-1}$ and $6.3 \times 10^{-5}\,cm^2\,s^{-1}$ were calculated for D_t in bulk solution, and $1.4 \times 10^{-5}\,cm^2\,s^{-1}$ and $1.2 \times 10^{-5}\,cm^2\,s^{-1}$ at the interface, in the absence and presence of lithium, respectively. These results for D_t in bulk solution agree with the experimental value of $1.33 \times 10^{-5}\,cm^2\,s^{-1}$ [51] obtained from conductivity measurements of dilute aqueous solutions at 298 K (taking into consideration the difference of temperature at which the simulation and experiments were performed and that the diffusion coefficient diminishes with the sodium concentration in aqueous solution[51]). From these results, we observe how the diffusion coefficient of sodium ions was almost unperturbed by the presence of lithium, although in both cases, with and without lithium, a decrease of more than 80% was estimated for D_t at the interface compared with the measurements in bulk solution.

This behavior may be explained by the way in which SDS is coordinated by lithium and sodium ions. Thus, Figure 11 shows the radial distribution g(r) of sodium and lithium ions around the sulphate and the esther oxygens of the SDS. From the height of the pecks and shapes of the radial distribution functions we can conclude that the presence of lithium hardly affected the coordination of sodium with the SDS, because lithium ions mainly coordinate with esther oxygens of the SDS, which are located at deepest zones of the aggregate, positions that are free to accept lithium, due to the fact that sodium ions are not able to reach these deep positions in the aggregate because their radius is bigger than that of lithium.

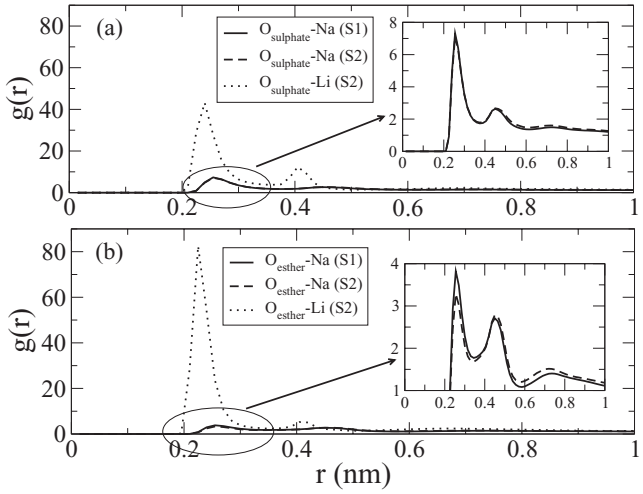

FIG. 11. Radial distribution function of sodium and lithium around sulphate and esther oxygens of the SDS, corresponding to the systems S1 (in the absence of lithium) and S2 (in the presence of lithium) in solution.

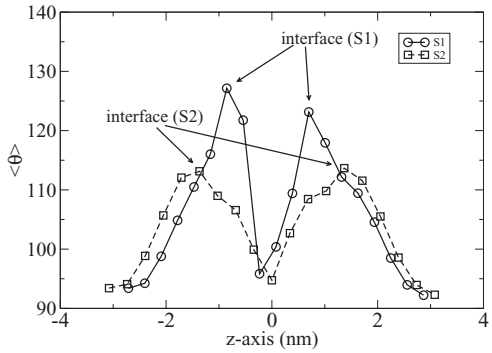

FIG. 12. Water dipole orientation from bulk water to the interior of the aggregate. The z-axis is perpendicular to the surface of the aggregate, and zero of the z-axis was placed in the middle of the aggregate.

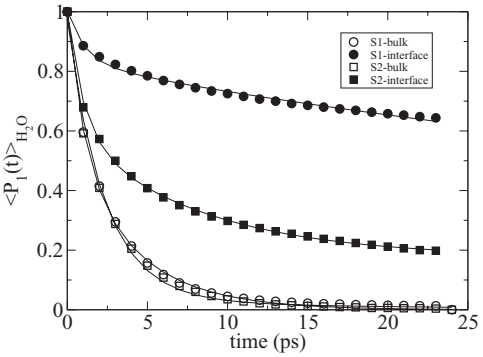

FIG. 13. $\langle P_1(t)\rangle$ calculated from simulation (points) and the solid line represents the fit to a multiexponential. For further information, see the text.

2. Orientation (θ) and reorientational relaxation time (τ) of water dipole

Figure 12 shows the orientation of the water dipole $\vec{\mu}$ with respect to the z-axis perpendicular to the surface of the aggregate, from bulk water to the interior of the aggregate. Note how the presence of lithium ions anchored to the SDS-heads contributes noticeably to the screening of the electrostatic interactions between the aggregate and the water molecules, by lowering the orientation of water dipole in the vicinity of the aggregate.

In line with this argument, to gain a precise insight into the dynamic behavior of water, the reorientational relaxation time of the water dipole was investigated. Dynamic properties associated with the water rotation can be extracted from correlation functions, such as the reorientational relaxation time of the water dipole, which is related with experimental measurements of the dielectric conductivity and the H-NMR relaxation times.[52] This relaxation property is an example of how water approaches the equilibrium from an arbitrary initial state. A characteristic of this process is that it is governed by the different type of particles and interactions that are there in the system. In this sense, the reorientational correlation time, τ_1, in liquids is studied by correlation functions $C_1(t)$ defined as

$$C_1(t) = \langle P_1(\vec{\mu}(t)\vec{\mu}(0))\rangle, \tag{5}$$

where $\vec{\mu}$ is the water unitary dipole vector, and P_1 is a first-order Legendre polynomial and $\langle\cdots\rangle$ denotes averaging over all the simulation. In this respect, $\langle P_1\rangle = \langle\vec{\mu}(t)\vec{\mu}(0)\rangle = \langle\cos(\xi)\rangle$, where ξ is the angle formed by the water unitary dipole vector at two different times separated by an elapsed time Δt.

On the other hand, in general, $\langle P_1(t)\rangle$ can be fitted by a multiexponential as follows:

$$\langle P_1(t)\rangle = \sum_{i=1}^{3} a_i e^{-\frac{t}{\tau_i}}, \tag{6}$$

where a_i is a constant of the fit associated with the time τ_i. Note that although a_i and τ_i change between fits, a reproducible apparent relaxation time, τ^{app}, can be obtained as follows:

$$\tau^{app} = \frac{\sum_{i=1}^{3} a_i\tau_i}{\sum_{i=1}^{3} a_i}. \tag{7}$$

Figure 13 shows $\langle P_1(t)\rangle$ obtained from simulation in the presence and absence of lithium ions, for the bulk solution and at the aggregate/solution interface. By fitting $\langle P_1(t)\rangle$ to the multiexponential, values of $\tau_b^{app} = 2.87$ ps and $\tau_i^{app} = 287$ ps for water in the S1 sample were estimated, in bulk solution (b) and at the interface (i), respectively. On the other hand, values of $\tau_b^{app} = 2.55$ ps and $\tau_i^{app} = 21.4$ ps were attained for the S2 sample. From these results, we observe that the reorientational dynamics of water in bulk solution agrees with the experimental data of 1.90 ps obtained from the nuclear magnetic resonance spin-lattice relaxation time proposed by Rahman and Stillinger[53] in bulk water. In addition, this value also agrees with that proposed by Wu *et al.* (1.17 ps) obtained from MD simulations with the SPC water model at a temperature of 298 K.[54] However, when we focus on the behavior of water in the vicinity of the interface, we observe that there is a substantial increase in the reorientational time, τ^{app}, reaching up to two orders of magnitude higher than in bulk solution in the case in the absence of lithium, while in the presence of lithium τ^{app} only increased by one order of magnitude. This difference in the rotational relaxation time at the interface may be related with the effectiveness of the screening associated with lithium, which reduces the electrostatic interactions of the aggregate with the dipole of the water in bulk solution. Consequently, a reduction in the rotational relaxation time for the water dipole is expected in the presence of lithium, in line with our simulation results.

IV. CONCLUSIONS

The study of discotic nematic lyotropic liquid crystals provides relevant information for understanding at a molecular level, much more complicated systems such as cell membranes. In this regard, the experimental study of these molecular aggregates showed that the presence of lithium did not affect the aggregate size compared with the size reached when only sodium was present. However, a decrease in the alignment of the aliphatic chains with respect to the magnetic field was observed. Thus, while Na^+ only partially

coordinated the aggregate at the interface, Li^+ mainly coordinated the amphiphilic molecules at the deepest positions of the aggregate, which are mainly occupied by the ester-oxygens of the SDS molecules. As a consequence of this remarkable difference in behavior between sodium and lithium ions, the steady and dynamic interfacial properties of the aggregate and water were greatly perturbed. Finally, because Li^+ accumulates at the interior of the interface, it might have important biophysical implications in the function of ionic channels, since substantial modifications in the lateral pressure of the lipid bilayer could occur, which could be related with the blockage of the ion transduction process across the cell membrane.

ACKNOWLEDGMENTS

The authors acknowledge the financial support from Fondecyt-Chile (Grant No. 1095175). V.E.B.-P. acknowledges a doctoral fellowship from Conicyt, the University of Chile, and Polytechnic University of Cartagena (UPCT), for financing a stay in Cartagena, Spain. The authors are grateful to the Computing Center of the UPCT (SAIT) for the technical support in carrying out the simulations presented in this work.

[1] G. Warr, F. Grieser, and D. Evans, J. Chem. Soc., Faraday Trans. **82**, 1829 (1986).
[2] T. Imae, R. Kamiya, and S. Ikeda, J. Colloid Interface Sci. **108**, 215 (1985).
[3] T. Yildiz and N. Kazanci, J. Mol. Struct. **886**, 158 (2008).
[4] A. Nesrullajev, F. Tepehan, and N. Kazanci, Mater. Chem. Phys. **73**, 74 (2002).
[5] R. Montecinos, H. Ahumada, R. Araya-Maturana, A. Olea, and B. Weiss-López, J. Colloid Interface Sci. **316**, 126 (2007).
[6] G. Colafemmina, R. Recchia, A. S. Ferrante, S. Amin, and G. Palazzo, J. Phys. Chem. B **114**, 7250 (2010).
[7] G. Ouriques, R. Sander, and V. Dmitriev, Langmuir **16**, 7900 (2000).
[8] A. Nesrullajev, N. Kazanci, and T. Yildiz, Mater. Chem. Phys. **80**, 710 (2003).
[9] V. Bahamonde, H. Ahumada, R. Araya-Maturana, and B. E. Weiss-López, Aust. J. Chem. **63**, 68 (2010).
[10] P. van der Schoot, V. Popa-Nita, and S. Kralj, J. Phys. Chem. B **112**, 4512 (2008).
[11] J. Lagerwall and G. Scalia, Curr. Appl. Phys. **12**, 1387 (2012).
[12] S. Schymura, E. Enz, S. Roth, G. Scalia, and J. Lagerwall, Synth. Met. **159**, 2177 (2009).
[13] X. Jiang, Y. Xie, J. Lu, L. Zhu, W. He, and Y. Qian, Chem. Mater. **13**, 1213 (2001).
[14] D. Son, A. Wolosiuk, and P. Braun, Chem. Mater. **21**, 628 (2009).
[15] *The Structure of Biological Membranes*, edited by P. Yeagle (CRC Press, Inc., 1991).
[16] C. Cade, Med. J. Aust. **2**, 349 (1949).
[17] J. Pettegrew, K. Panchalingam, R. McClure, S. Gershon, L. R. Muenz, and J. Levine, Bipolar Disord. **3**, 189 (2001).
[18] A. Strunecka, J. Patocka, and M. Sarek, J. Appl. Biomed. **3**, 25 (2005).
[19] J. Pettegrew, J. Short, R. Woessner, S. Strychor, D. McKeag, J. Armstrong, N. Minshew, and A. Rush, Biol. Psychiatry **22**, 857 (1987).
[20] P. Bhalla, P. Nair, M. Garg, and D. K. Dhawan, Toxicol. Environ. Chem. **91**, 723 (2009).
[21] L. Carbonell, M. Cuffi, and J. Forn, Eur. Neuropsychopharmacol. **14**, 497 (2004).
[22] M. Suwalsky, P. Fierro, F. Villena, and C. Sotomayor, Biophys. Chem. **129**, 36 (2007).
[23] C. J. Buttler-Munro, "Membrane target of lithium in cortical neurons in vitro," Ph.D. thesis (University of Otago, Dunedin, New Zealand, 2011), http://hdl.handle.net/10523/560.
[24] N. Turro and A. Yekta, J. Am. Chem. Soc. **100**, 5951 (1978).
[25] R. Montecinos, H. Ahumada, R. Martínez, F. Olea, R. Araya-Maturana, M. Aliste, D. Tieleman, and B. Weiss-Lopez, Langmuir **20**, 5703 (2004).
[26] R. Alargova, I. Kochijashky, M. Sierra, and R. Zana, Langmuir **14**, 5412 (1998).
[27] H. J. C. Berendsen, D. van der Spoel, and R. van Drunen, Comput. Phys. Commun. **91**, 43 (1995).
[28] E. Lindahl, B. Hess, and D. van der Spoel, J. Mol. Model. **7**, 306 (2001).
[29] T. Darden, D. York, and L. Pedersen, J. Chem. Phys. **98**, 10089 (1993).
[30] U. Essmann, L. Perera, M. Berkowitz, T. Darden, H. Lee, and L. Pedersen, J. Chem. Phys. **103**, 8577 (1995).
[31] B. Hess, H. Bekker, H. Berendsen, and J. Fraaije, J. Comput. Chem. **18**, 1463 (1997).
[32] H. Berendsen, J. Postma, W. van Gunsteren, A. DiNola, and J. Haak, J. Chem. Phys. **81**, 3684 (1984).
[33] J. Pople and G. Segal, J. Chem. Phys. **44**, 3289 (1966).
[34] M. J. Frisch, G. W. Trucks, H. B. Schlegel *et al.*, GAUSSIAN 03, Revision B.03, Gaussian, Inc., Pittsburgh, PA, 2003.
[35] B. Besler, K. Merz, and P. Kollman, J. Comput. Chem. **11**, 431 (1990).
[36] B. Jonsson, O. Edholm, and O. Teleman, J. Chem. Phys. **85**, 2259 (1986).
[37] E. Egberts, S. Marrink, and H. Berendsen, Eur. Biophys. J. Biophys. Lett. **22**, 423 (1994).
[38] P. Ahlstrom and H. Berendsen, J. Phys. Chem. **97**, 13691 (1993).
[39] J. López Cascales, J. García de la Torre, S. Marrink, and H. Berendsen, J. Chem. Phys. **104**, 2713 (1996).
[40] D. Poger, W. F. van Gunsteren, and A. E. Mark, J. Comput. Chem. **31**, 1117 (2010).
[41] T. Heinz, W. van Gunsteren, and P. Hünenberger, J. Chem. Phys. **115**, 1125 (2001).
[42] W. van Gunsteren and H. Berendsen, *GROMOS: GROningen MOlecular Simulation is a Software Package* (Biomos, Nijenborgh 4, 9747AG Groningen, The Netherlands, 1987).
[43] H. Berendsen, J. Postma, W. van Gunsteren, and J. Hermans, *Intermolecular Forces* (D. Reidel Publishing Company, 1981).
[44] A. Nesrullajev, Mater. Chem. Phys. **123**, 546 (2010).
[45] K. Hiltrop, *Lyotropic Liquid Crystals in Topics in Physical Chemistry* (Springer, New York, 1994), Vol. 3.
[46] A. Abragam, *Principles of Nuclear Magnetism* (Oxford University Press, 1985).
[47] H. Hauser and G. Shipley, Biochemistry **22**, 2171 (1983).
[48] J. López Cascales and J. de la Torre, Biochim. Biophys. Acta-Biomembr. **1330**, 145 (1997).
[49] A. Seelig and J. Seelig, Biochemistry **13**, 4839 (1974).
[50] J. Mähler and I. Persson, Inorg. Chem. **51**, 425 (2012).
[51] *CRC Handbook of Chemistry and Physics, Internet Version 2007*, 87th ed., edited by David R. Lide (CRC Press, Inc., 2007).
[52] R. Jellema, J. Bulthuis, and G. van der Zwan, J. Mol. Liq. **73–74**, 179 (1997).
[53] A. Rahman and F. Stillinger, J. Chem. Phys. **55**, 3336 (1971).
[54] Y. Wu, H. Tepper, and G. Voth, J. Chem. Phys. **124**, 024503 (2006).